J Mater Sci: Mater Electron (2023) 34:2059

Thermally stable multi-color emitting Dy^{3+}/Eu^{3+} co-doped $BaO–ZnO–Li_2O–P_2O_5$ glasses for w-LEDs

Kartika Maheshwari[1,2], Aman Prasad[3], Ravita Pilania[4], Shaik. Mahamuda[5], Yasha Tayal[1,2], and A. S. Rao[1,*]

[1] *Department of Applied Physics, Delhi Technological University, Bawana Road, Delhi 110042, India*
[2] *ABES Engineering College, Ghaziabad 201009, India*
[3] *Department of Physics and Computer Science, Dayalbagh Educational Institute (DEI), Agra 282002, India*
[4] *Department of Physics, Chaudhary Bansilal University, Bhiwani 127021, India*
[5] *Department of Engineering Physics, College of Engineering, Koneru Lakshmaiah Education Foundation, Vaddeswaram 522302, India*

Received: 10 July 2023
Accepted: 25 September 2023

ABSTRACT

Dy^{3+} and Dy^{3+}/Eu^{3+} co-doped $BaO–ZnO–Li_2O–P_2O_5$ (BZLP) glasses have been prepared and studied for their luminescence properties. Dy^{3+}doped BZLP glass emits red ($^4F_{9/2} \rightarrow {}^6H_{13/2}$), green ($^4F_{9/2} \rightarrow {}^6H_{15/2}$) and blue ($^4F_{9/2} \rightarrow {}^6H_{11/2}$) emission under 350 nm excitation. Doping of Eu^{3+} tunes the emission from Dy^{3+} in the BZLP glasses. The cool white emission shifts towards the warm white region at 350 nm excitation wavelength owing to the energy transfer between sensitizer Dy^{3+} and activator Eu^{3+} ions. Also, Dy^{3+}/Eu^{3+} co-doped BZLP glass gives intense red emission under 393 nm excitation. Dexter's theory was used to ascertain the energy transfer mechanism among the sensitizer Dy^{3+} and activator Eu^{3+} ions via Reisfeld's approximation. The glasses have significant thermal stability and high activation energy. These Dy^{3+}/Eu^{3+} co-doped BZLP glasses can be utilized in the fabrication of cool/warm w-LEDs and red emitting devices applications.

1 Introduction

Demand for energy is ever increasing. So, energy saving has become a very important research field being considered significantly [1, 2]. In artificial lighting, white light-emitting diodes (w-LEDs) lighting sources have become particularly important for reducing the world's energy consumption due to advantages like huge amount of energy saving, superior efficacy, compact size, environmental friendliness, etc. related to fluorescent lamps [3–5]. A commercial w-LED is based on a blue LED and YAG: Ce^{3+} phosphor [6, 7]. These w-LEDs suffer from low color rendering index, inappropriate color temperature and halo effect [8]. Glasses doped with transition ions have attracted considerable interest because of their memory and photoconducting properties. They also find potential applications in the development of new tunable solid-state lasers, solar-energy converters and fiber-optic communication devices [9]. To improve these shortcomings, the development of rare earth-activated glasses as a worthy substitute for phosphors is being investigated [8]. Furthermore, glass has many distinctive characteristics such as an

Address correspondence to E-mail: drsrallam@gmail.com

https://doi.org/10.1007/s10854-023-11394-7
Published online: 31 October 2023

easy cost-effective production process, good thermal and chemical stability along with a high value of rare earth solubility [10, 11].

The choice of a good glass host activated with rare earth ions is still a difficult task in assessing optical and lasing characteristics efficiently [12]. Numerous glass hosts like borates, tellurites, silicates, fluorides, phosphates etc. have been prepared and inspected for innumerable optical features. Phosphate is one of the appropriate glass hosts having distinguished properties like low melting temperature, highly thermally stability, high rare earth (RE) solubility, low dispersion and clear visibility in the wide-ranging spectrum [13, 14]. Phosphate glasses have found usage in the area of photonics but their hygroscopic nature and poor chemical stability limit their utility [15]. So, network modifiers (BaO, Li_2O) and an intermediate compound (ZnO) are added to the host thereby enhancing chemical & thermal stability and reducing thermal expansions. Additionally, ZnO helps reduce the hygroscopic affinity of the glass and increases rare earth ion solubility in the glass matrix. RE doped phosphate glasses improve the luminescent characteristics of materials in various fields such as optoelectronic devices and lasers due to the emission from the ultraviolet region to the infra-red region [16–21].

Trivalent lanthanide ions are considered the most appropriate activator in many crystalline or amorphous inorganic host lattices. Among the lanthanides, the trivalent Dy^{3+} is an important ion, which emits in the blue, yellow and red regions under numerous excitations. Through combination of these color, Dy^{3+} ion doped luminescent material is able to produce white lights. The white light is tuned by a proper yellow to blue ratio that can be altered by varying Dy^{3+} ions doping concentration [22, 23]. The bluish white light emitted from the Dy^{3+} ions doped glasses lacks a red constituent and also has high co-related color temperature (CCT). This cool bluish light can be tuned to warm white light via co-doping of appropriate rare earth ions that can emit in the red region. Various RE ions such as Dy^{3+}/Ce^{3+}, Dy^{3+}/Eu^{3+}, Dy^{3+}/Tm^{3+} etc. are being used to obtain proper artificial white light [24–26]. We have introduced red emitting Eu^{3+} ion as a co-activator in Dy^{3+} doped glass compositions so as to improve the CCT and generate warm white light. This was undertaken due to the overlapping of Dy^{3+} emission profile with Eu^{3+} ions excitation profile. This fact shows that some energy transfer can occur between both ions in the proposed phosphate glass composition [27].

In the current investigation, Dy^{3+}/Eu^{3+} activated BZLP glasses have been prepared to achieve the optimal energy transfer with thermal stability for warm white light generation and usage in other solid-state artificial lighting devices. Structural analysis along with the study of optical properties of the BZLP glasses has been undertaken in this research work.

2 Materials and methods

2.1 Preparation of Dy^{3+} and Dy^{3+}/Eu^{3+} induced BZLP glasses

Transparent RE ions doped glasses have been prepared via melt quenching routes with the help of highly pure reagents using the following chemical equations:

$$(15-x)\,BaO-15ZnO-10Li_2O-60P_2O_5 : xDy_2O_3\left(x\text{varies from 0.1 to 2.0 mol\% concentration of } Dy^{3+}\text{ions}\right)$$

$$(15-y)\,BaO-15ZnO-10Li_2O-60P_2O_5 : yEu_2O_3\left(y = 0.1\text{ mol\% concentration of } Eu^{3+}\text{ions}\right)$$

Besides the aforementioned glasses, a series of Dy_2O_3 and Eu_2O_3 co-doped glasses was also prepared:

(15-x–y) BaO-15ZnO-10Li_2O-60P_2O_5:$x$$Dy_2O_3$:$y$$Eu_2O_3$ (x = 1.5 mol% concentration of Dy^{3+} ions and y = 0.0, 1.0, 2.0, 3.0, 4.0 and 5.0 mol% of Eu^{3+} ions). The prepared Dy^{3+}/Eu^{3+} co doped glass samples of size 3 cm and uniform thickness 2 mm were named as BZLP:DE0, BZLP:DE1, BZLP:DE2, BZLP:DE3, BZLP:DE4 and BZLP:DE5 and shown in the Fig. 1.

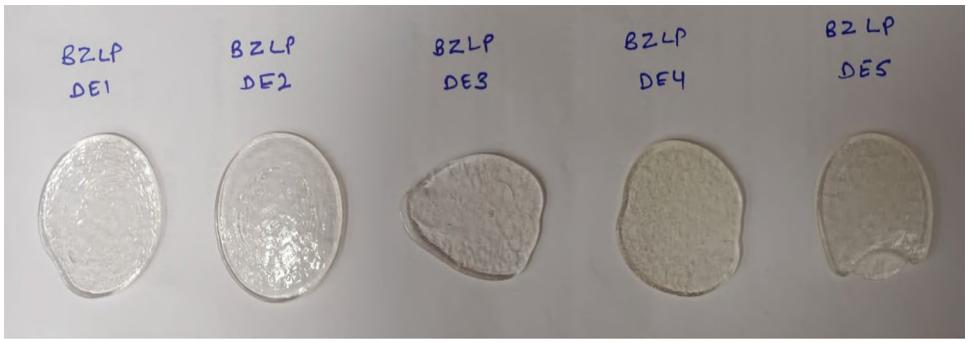

Fig. 1 Dy^{3+}/Eu^{3+}co-doped ions BZLP glass samples

Appropriate stoichiometric amounts of $BaCO_3$, ZnO, Li_2CO_3, $NH_4H_2PO_4$ and Dy_2O_3 were taken and ground for 1 h and the blended mixture was further heated in a furnace for melting at 1200 °C. After a while, the powder mixture turned into a liquid. This liquid mix was then immediately quenched on a preheated brass plate to give the final glass product of uniform thickness. Further, the prepared glasses were annealed at 350 °C for 1 h to remove thermal shock and air bubbles strain. These glasses were polished with emery paper with 40 grit and also used red oxide powder so that the smoothness of the glass does not be affected.

2.2 Instrumentation

XRD data of Dy^{3+}/Eu^{3+} co-doped BZLP glass was recorded using a D8 advance Bruker X-ray diffractometer in the $10° \leq 2\theta \leq 80°$ range. The absorption profile was recorded via JASCO V 670 spectrophotometer. Photoluminescence (PL) studies were carried out in a JASCO 8300FL Spectro fluorophotometer at room temperature. The decay profile co-doped BZLP glass has been characterized using an Edinburgh FLS980 spectrophotometer. Temperature-dependent PL (TD-PL) profiles were recorded using ocean optics spectrophotometer (FLAME- S-XR1-ES).

3 Results and discussions

3.1 Structural analysis

The amorphous nature of the prepared Dy^{3+}/Eu^{3+} co-doped BZLP glass has been analysed using the recorded XRD profile as shown in Fig. 2. The profile contains a wide band with the nonexistence of any

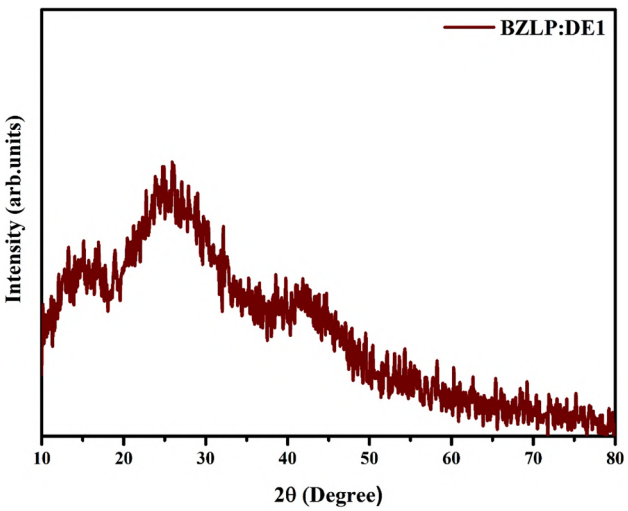

Fig. 2 XRD pattern of Dy^{3+}/Eu^{3+}co-doped BZLP glass

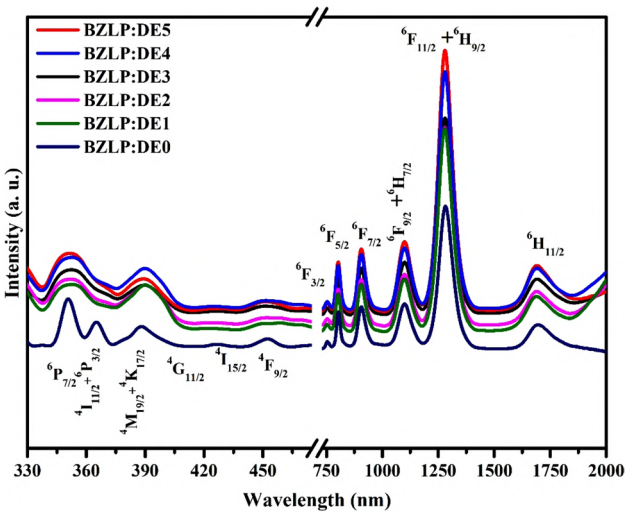

Fig. 3 Absorption profile of Dy^{3+} doped and Dy^{3+}/Eu^{3+}co-doped BZLP glasses

sharp peaks, confirming the prepared Dy^{3+}/Eu^{3+} co-doped BZLP glasses having glassy and amorphous in nature.

3.2 Absorption characteristics

The absorption profiles of Dy^{3+} doped BZLP glasses in 330–2000 nm range have been shown in Fig. 3. Peaks pertaining to transitions from $^6H_{15/2}$ state to many higher energy levels at $^6P_{7/2}$,$^4I_{11/2}$ + $^6P_{3/2}$,$^4M_{19/2}$ + $^4K_{17/2}$, $^4G_{11/2}$,$^4I_{15/2}$, $^4F_{9/2}$,$^6F_{3/2}$, $^6F_{5/2}$, $^6F_{7/2}$,$^6F_{9/2}$ + $^6H_{7/2}$,$^6F_{11/2}$ + $^6H_{9/2}$ and $^6H_{11/2}$ of Dy^{3+} ions [20]. The absorption peak due to $^6H_{15/2}$ to $^6F_{11/2}$ + $^6H_{9/2}$ transition is most intense and follows $|\Delta S| = 0$, $|\Delta L| \leq 2$ and $|\Delta J| \leq 2$ [28].

The absorption characteristics of Dy^{3+}/Eu^{3+} co-doped BZLP glasses were also illustrated in Fig. 3. The bands are mainly due to Dy^{3+} ions and broaden in the UV region, when co-doped with Eu^{3+} ions as depicted in Fig. 3. The absorption peaks observed for Dy^{3+} doped BZLP glass in infrared region were in good agreement with the literature [6, 7, 15].

On the basis of absorption characteristics, optical band gap of all prepared glasses was evaluated via Davis and Mott relation as follows [29]:

$$\alpha h\nu = B\left(h\nu - E_{opt}\right)^{n}$$

Here E_{opt} is indirect energy bandgap, α represents the absorption coefficient, B is the band trailing parameters and $h\nu$ is incident photon energy. The value of n is 2 for indirect allowed transitions [30]. As per the plot presented in Fig. 4, estimated indirect E_{opt} values are 4.21, 4.04, 3.96, 3.91, 3.88 and 3.86 eV for BZLP:DE0, BZLP:DE1, BZLP:DE2, BZLP:DE3, BZLP:DE4 and BZLP:DE5 glasses, respectively.

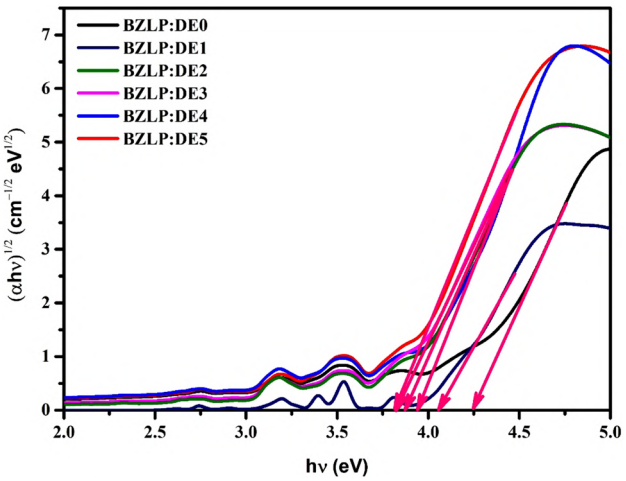

Fig. 4 Indirect bandgap plot of Dy^{3+} doped and Dy^{3+}/Eu^{3+}co-doped BZLP glasses

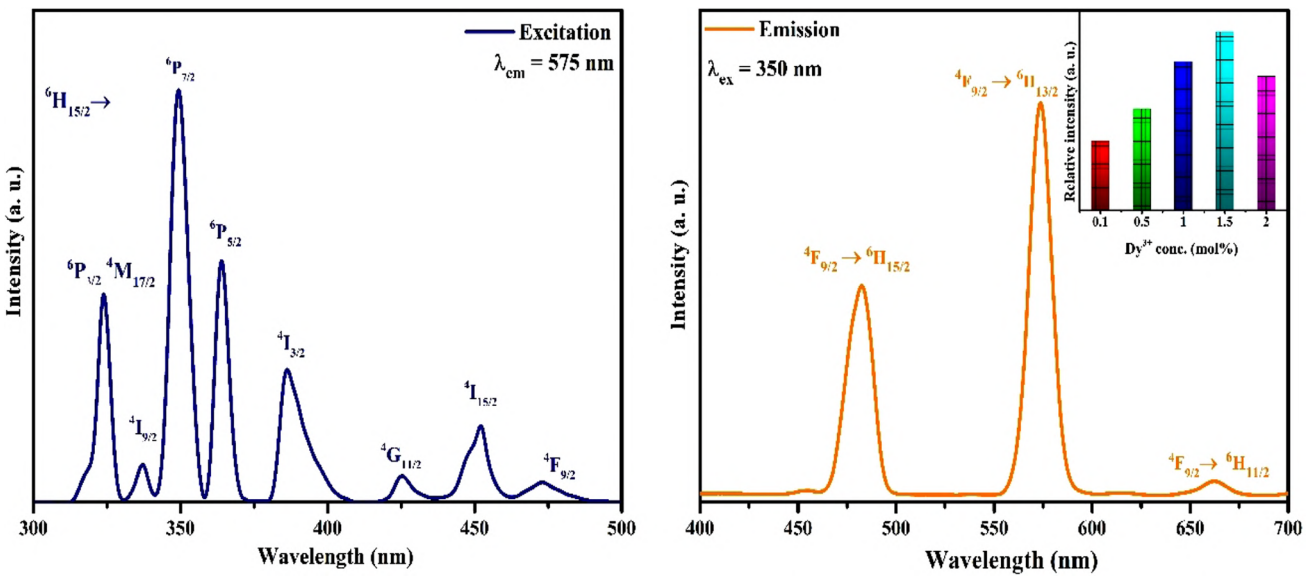

Fig. 5 Excitation and emission spectrum of Dy^{3+} doped BZLP glass at λ_{em} = 575 and λ_{ex} = 350 nm respectively. The inset plot represents the change in emission intensity with Dy^{3+} ions concentration in BZLP glasses

3.3 PL study of singly doped Dy^{3+} ions in BZLP glasses

PL characteristics of 0.1 mol% Dy^{3+} doped BZLP glass was presented in Fig. 5. PL excitation spectrum with monitoring the 575 nm emission wavelength contains various peaks in 300–500 nm range. The excitation peaks were observed at 322, 337, 350, 362, 386, 425, 449 and 473 nm corresponding transitions are mentioned in Fig. 5. Amongst the excitation peaks, the dominant peak at 350 nm ($^6H_{15/2} \rightarrow {}^6P_{7/2}$) transition was chosen as the excitation wavelength to record the emission characteristics [31, 32].

Figure 5 shows the emission spectrum of 0.1 mol% Dy^{3+} doped BZLP glass under the excitation of 350 nm wavelength. The emission spectrum exhibits the blue, yellow and red peaks at 483 nm ($^4F_{9/2} \rightarrow {}^6H_{15/2}$), 575 nm ($^4F_{9/2} \rightarrow {}^6H_{13/2}$) and 661 nm ($^4F_{9/2} \rightarrow {}^6H_{11/2}$). The nature of transitions $^4F_{9/2} \rightarrow {}^6H_{15/2}$ and $^4F_{9/2} \rightarrow {}^6H_{13/2}$ is magnetic dipole and forced electric dipole respectively. The $^4F_{9/2} \rightarrow {}^6H_{11/2}$ transition, on the other hand, is both magnetic as well as in forced electric in nature [33]. The ($^4F_{9/2} \rightarrow {}^6H_{13/2}$) transition is the leading the all-emission peaks. Further, the emission intensity can depend on the doping concentrations. Hence the doping concentration of Dy^{3+} ion was optimized by preparing a series of glass with 0.1 to 2.0 mol% of Dy^{3+} ions. The inset shows the variation in emission intensity with increasing Dy^{3+} concentration. The emission intensity upsurges till 1.5 mol% of Dy^{3+} and then declines [34]. This was due to mutual interactions and resonant energy transfer among the doping ions in BZLP i.e., concentration quenching effect [34]. On the basis of the emission profile, the 1.5 mol% is the optimized concentration of Dy^{3+} ions in BZLP glasses.

3.4 PL study of singly doped Eu^{3+} ions in BZLP glasses

Figure 6 shows the luminescence profile of Eu^{3+} doped BZLP glass at $\lambda_{em} = 612$ and $\lambda_{ex} = 393$ nm respectively. The excitation profile shows a number of peaks in 300–500 nm range owing to the ($^7F_0 \rightarrow {}^5H_6$), ($^7F_0 \rightarrow {}^5D_4$), ($^7F_0 \rightarrow {}^5L_7$), ($^7F_0 \rightarrow {}^5L_6$), ($^7F_0 \rightarrow {}^5D_3$) and ($^7F_0 \rightarrow {}^5D_2$), Eu^{3+} ions transitions. Amongst the several excitations, the dominant peak was observed at 393 nm corresponding to $^7F_0 \rightarrow {}^5L_6$ transition. Emission profile is illustrated in 500–750 nm range at $\lambda_{ex} = 393$ nm in the same figure. The emission profile shows numerous sharp peaks attributed to ($^5D_0 \rightarrow {}^7F_0$), ($^5D_0 \rightarrow {}^7F_1$), ($^5D_0 \rightarrow {}^7F_2$), ($^5D_0 \rightarrow {}^7F_3$), and ($^5D_0 \rightarrow {}^7F_4$) Eu^{3+} ions transitions. The transitions $^5D_0 \rightarrow {}^7F_1$ and $^5D_0 \rightarrow {}^7F_2$ of Eu^{3+} ions can be characterised as magnetic and forced electric dipole in nature, respectively. The dominant emission peak was situated at 612 nm under 393 nm excitation [35].

3.5 PL study of co-doped BZLP:Dy^{3+}/Eu^{3+} glasses

The excitation spectra of Dy^{3+}/Eu^{3+} co-doped BZLP glass (BZLP:DE1) were recorded by monitoring the emission wavelengths at 575 and 612 nm as

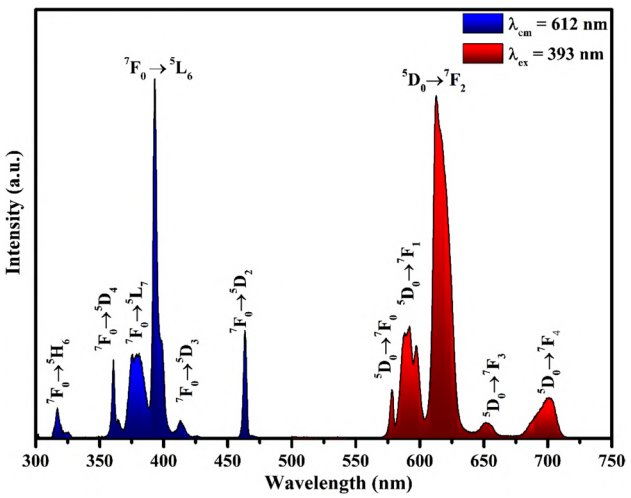

Fig. 6 Excitation and emission spectrum of 1.0 mol% Eu^{3+} doped BZLP glass at $\lambda_{em} = 612$ and $\lambda_{ex} = 393$ nm respectively

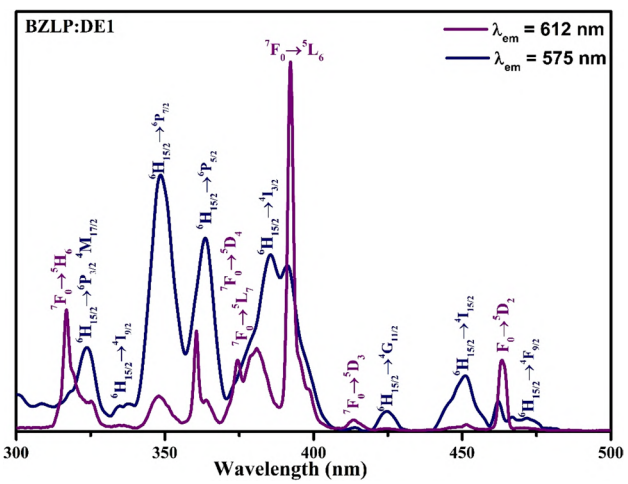

Fig. 7 Excitation spectra of BZLP:DE1 glass at $\lambda_{em} = 575$ and 612 nm

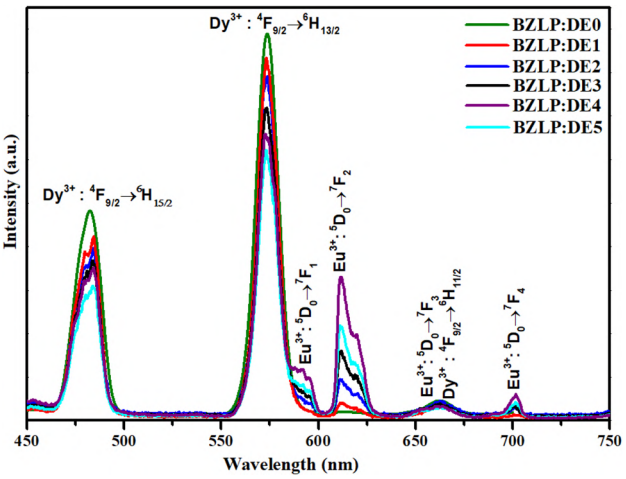

Fig. 8 Emission spectra of Dy^{3+}/Eu^{3+}co-doped BZLP glasses at $\lambda_{ex} = 350$ nm

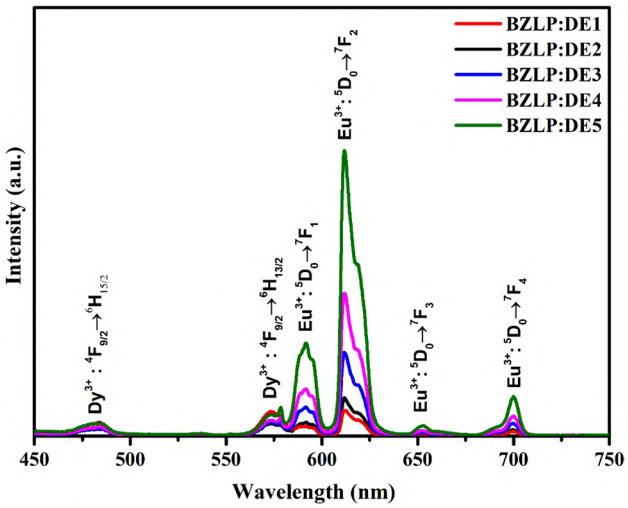

Fig. 9 Emission spectra of Dy^{3+}/Eu^{3+}co-doped BZLP glasses at $\lambda_{ex} = 393$ nm

illustrated in Fig. 7. The excitation profile by monitoring the emission wavelength at 575 nm exhibits a number of excitation peaks in 300–500 nm range, owing to the transition from $^6H_{15/2}$ to $^6P_{3/2}$, $^4M_{17/2}$, $^4I_{9/2}$, $^6P_{7/2}$, $^6P_{5/2}$, $^4I_{3/2,}$ $^4G_{11/2}$, $^4I_{15/2}$ and $^4F_{9/2}$ of Dy^{3+} ions. Also, some additional peaks were detected at 393 and 465 due to the $^7F_0 \rightarrow {}^5L_6$ and $^5D_2$ transitions of Eu^{3+} ions. The occurrence of excitation peaks related to Eu^{3+} ions while monitoring the Dy^{3+} ions emission peaks suggested that the Dy^{3+} plays an important role in energy transfer to the Eu^{3+} ion. The excitation profile while monitoring 612 nm emission exhibits excitation peaks due to the $^7F_0 \rightarrow {}^5H_6$, $^5D_4$, $^5L_7$, $^5L_6$, $^5D_3$ and $^5D_2$, transitions of Eu^{3+} ions. The overlap of the excitation spectra of BZLP: DE1 confirms the ability of the glass to be excited by n-UV radiation.

Dy^{3+}/Eu^{3+} co-doped glasses were excited by 350 nm wavelength and the corresponding emission spectra are shown in Fig. 8. The emission profile changes with increasing content of Eu^{3+} ions in the glasses. The peak intensity related to $^4F_{9/2} \rightarrow {}^6H_{15/2}$, $^6H_{13/2}$ and $^6H_{11/2}$ transitions of Dy^{3+} reduces with increasing Eu^{3+} ions content whereas new peaks attributed to $^5D_0 \rightarrow {}^7F_1$, $^7F_2$, $^7F_3$, and $^7F_4$ transitions of Eu^{3+} ions are observed in the spectra. The reduction in Dy^{3+} emission peak intensity and simultaneous enrichment in the Eu^{3+} ions emission intensity signifies energy transfer between sensitizer Dy^{3+} and activator Eu^{3+} ions [36].

Furthermore, the PL spectra of Dy^{3+}/Eu^{3+} co-doped BZLP glasses were recorded under 393 nm excitation as revealed in Fig. 9. Numerous emission peaks situated at 591($^5D_0 \rightarrow {}^7F_1$), 612 ($^5D_0 \rightarrow {}^7F_2$), 651($^5D_0 \rightarrow {}^7F_3$) and 700 ($^5D_0 \rightarrow {}^7F_4$) nm of Eu^{3+} ion can be seen. Apart from this, two peaks were also detected at 483 and 575 nm corresponding to $^4F_{9/2} \rightarrow {}^6H_{15/2}$ and $^6H_{13/2}$ transitions of Dy^{3+} ions, respectively. Peaks corresponding to Eu^{3+} ion transitions are more intense than those of Dy^{3+} ion transitions. The intensity of $^5D_0 \rightarrow {}^7F_1$,$^7F_2$, $^7F_3$,$^7F_4$ transitions enhances with increase in Eu^{3+} ions, whereas minute changes are observed in emission related with to $^4F_{9/2} \rightarrow {}^6H_{15/2}$, $^6H_{13/2}$ transitions of Dy^{3+} ions. Thus, Dy^{3+} ions sensitize Eu^{3+} ions as is evident from PL studies and transfer a part of absorbed energy which is converted to visible emission [37, 38].

A partial energy level diagram of Dy^{3+} and Eu^{3+} ions is shown in Fig. 10 to realize the sensitizer and activator ions energy transfer process. Dy^{3+} and Eu^{3+} ions get excited to upper energy levels by n-UV radiation and then fall to lower energy states via non-radiative decay. Subsequently, the Dy^{3+} ions give emissions at 483, 575 and 661 nm ascribed to the $^4F_{9/2} \rightarrow {}^6H_{15/2}$, $6H_{13/2}$ and $^6H_{11/2}$ transitions whereas Eu^{3+} emits owing to $^5D_0 \rightarrow {}^7F_1$, $^7F_2$, $^7F_3$, and $^7F_4$ transitions. Some energy is also shifted from Dy^{3+} to Eu^{3+} ions along with the individual emissions. The energy shifting takes place as the energy level $^4I_{15/2}$ of Dy^{3+} ion is above the $^5D_{2,}$ $^5D_1$ and $^5D_0$ energy levels of Eu^{3+}

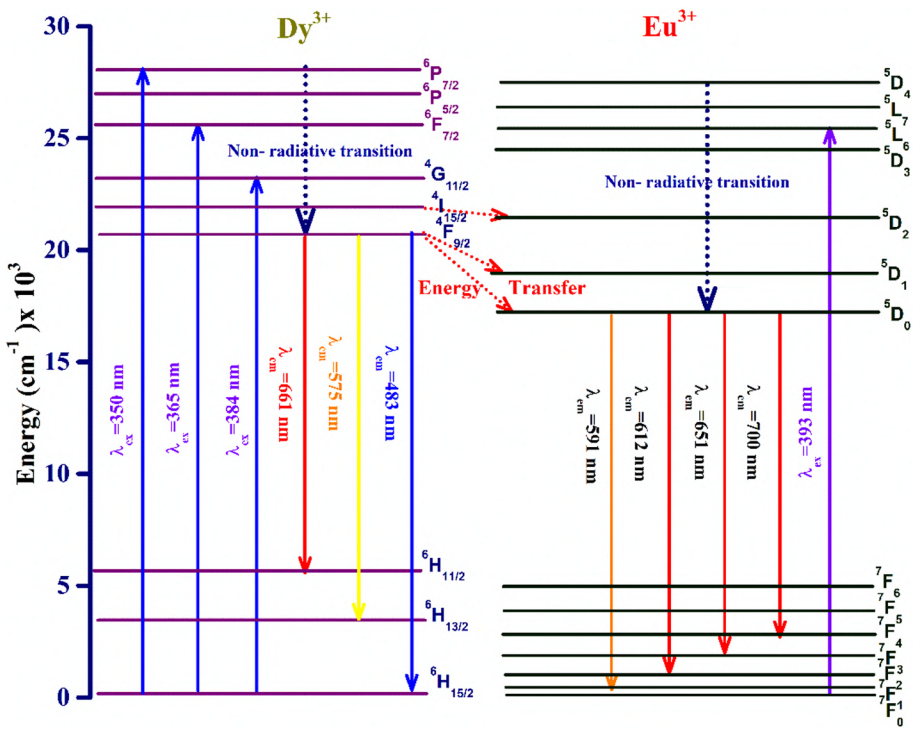

Fig. 10 Partial energy level diagram of Dy^{3+} and Eu^{3+} ions in BZLP glasses

ion. Also, the $^4F_{9/2}$ level of Dy^{3+} lies above the $^5D_1$ and $^5D_0$ levels of Eu^{3+} ions. Owing to the less energy difference between these levels, a part of absorbed energy from Dy^{3+} ions migrate to the Eu^{3+} ions in BZLP glasses as seen in PL spectra.

Mainly multipolar exchange interaction type of energy transfer takes places in rare earth doped glasses, which can be categorized into three ways of interaction i.e., quadrupole–quadrupole, dipole–dipole and dipole-quadrupole. The types of energy transfer among the nearest doped ions were analysed via Dexter's multipolar exchange interaction expression with Reisfeld's approximation as follows [39]:

$$\frac{\eta_0}{\eta} \propto C^{n/3} \tag{1}$$

η_0 and η symbolize the radiant quantum efficiency of sensitizer Dy^{3+} ions in the absence of an activator and quantum efficiency of sensitizer Dy^{3+} ions with Eu^{3+} (activator), respectively. C signifies the sum of concentration of dopant ions. The nature of multipolar exchange interaction is indicated by n in the equation above. Depending whether the interaction is dipole–dipole, dipole-quadrupole and quadrupole–quadrupole, the value of n can be 6, 8, or 10 respectively. The radiation intensities are linked to the ratio between η_0 and η as shown below [40]:

$$\frac{I_{SO}}{I_s} \propto C^{n/3} \tag{2}$$

In the above equation, I_{SO} signifies emission intensity of Dy^{3+} doped glass and I_S represent the emission intensity of Dy^{3+}/Eu^{3+}co-doped glass. The graphs of I_{SO}/I_S versus $C^{n/3}$ taking n = 6, 8, 10 can be seen in Fig. 11. The non-radiative, dipole-to-dipole character of the interaction and energy transfer between the rare earth ions was confirmed by the best linear fit, which was found for n = 6.

3.6 Lifetime and energy transfer analysis

The lifetime curves of Dy^{3+}/ Eu^{3+}co-doped BZLP glasses were recorded at λ_{em} = 572 nm under excitation λ_{ex} = 350 nm and shown in Fig. 12. The lifetime curves are exponential in nature and can be fitted with bi-exponential function as given below [41]:

$$I = I_0 + A_1 exp\left(-\frac{t}{\tau_1}\right) + A_2 exp\left(-\frac{t}{\tau_2}\right) \tag{3}$$

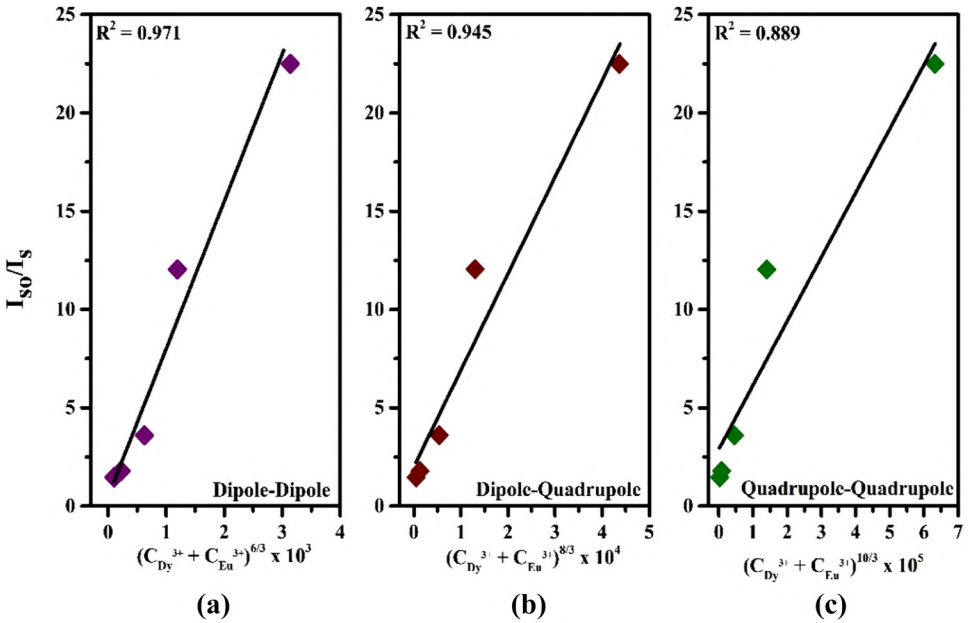

Fig. 11 Plot between I_{SO}/I_S versus (a) $(C_{Dy+Eu})^{6/3}$, (b)$(C_{Dy+Eu})^{8/3}$ and (c)$(C_{Dy+Eu})^{10/3}$

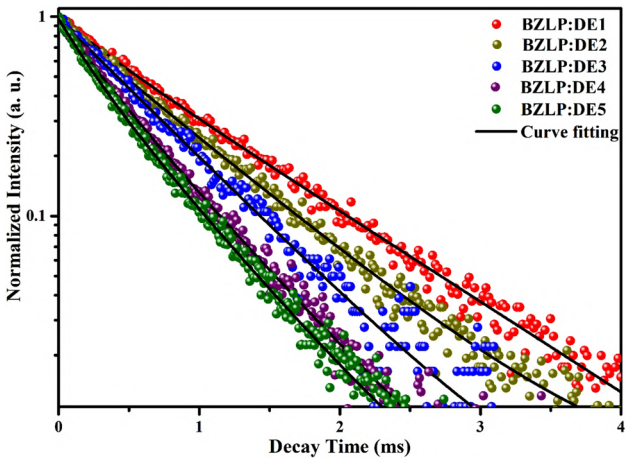

Fig. 12 Decay curves of Dy^{3+}/Eu^{3+}co-doped BZLP glasses at $\lambda_{ex}=350$ & $\lambda_{em}=575$ nm

Here I and I_0 denote the emission intensity at any instant t and t = 0, respectively and τ_1 and τ_2 denote the slow and fast decay components. A_1 and A_2 denote the fitting constants. On the basis of these parameters, the average lifetime (τ_{avg}) were calculated using the formula as mentioned [42]:

$$\tau_{avg} = \frac{A_1\tau_1^2 + A_2\tau_2^2}{A_1\tau_1 + A_2\tau_2} \tag{4}$$

The evaluated τ_{avg} values for the prepared Dy^{3+}/Eu^{3+}co-doped BZLP glasses are tabulated in Table 1. The occurrence of energy transfer between the dopant ions is confirmed by the decrease in the τ_{avg} values with increasing Eu^{3+} concentration. η_T is the energy transfer efficiency probability given as [43]:

$$\eta_T = 1 - \frac{\tau_d}{\tau_{d0}} \tag{5}$$

Table 1 CIE color coordinates (*x, y*), CCT (K), lifetime, Dy^{3+} to Eu^{3+} energy transfer efficiency of prepared co-doped BZLP glasses at $\lambda_{ex}=350$ and $\lambda_{em}=575$ nm

Sample name	CIE coordinates (*x, y*)	CCT (K)	Decay time (μs)	Energy transfer efficiency η_T(%)
BZLP:DE0	(0.372, 0.424)	4474	589	–
BZLP:DE1	(0.383, 0.410)	4125	571	3.05
BZLP:DE2	(0.376, 0.416)	4340	543	7.80
BZLP:DE3	(0.378, 0.405)	4185	524	11.03
BZLP:DE4	(0.383, 0.394)	3432	504	14.43
BZLP:DE5	(0.402, 0.391)	3180	496	15.78

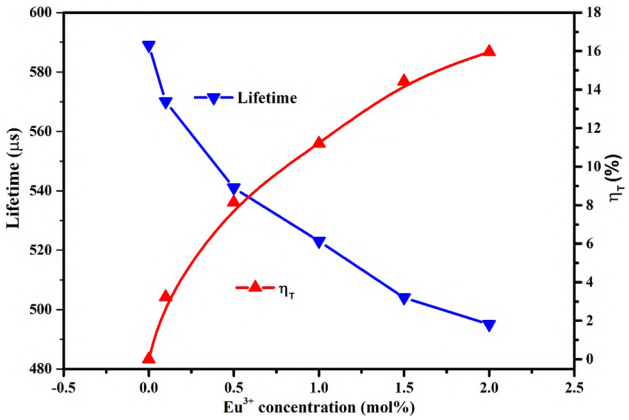

Fig. 13 Variation in lifetime and ET efficiency with Eu^{3+} ions concentration in Dy^{3+}/Eu^{3+}co-doped BZLP glasses

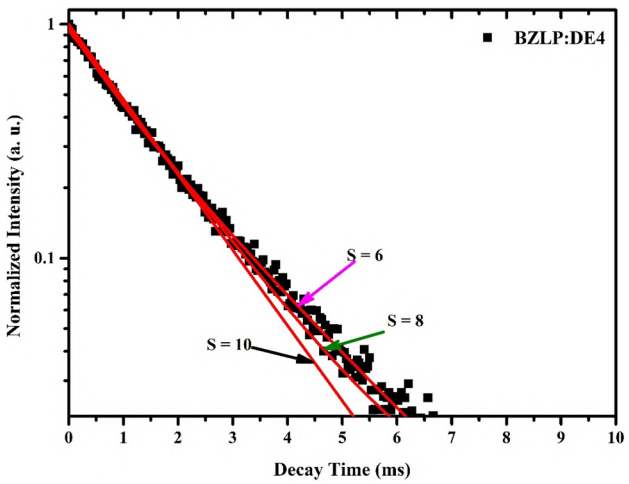

Fig. 14 I-H fitted decay curves of BZLP:DE4 glass

Here τ_d and τ_{d0} denote the lifetime of the co-doped and singly doped glasses respectively. Table 1 provides a tabulation of the energy transfer probability (η_T) parameter as well. It can be seen that when concentration of Eu^{3+} ions increases, η_T increases as well. The likelihood of energy transfer seems to increase by five times for an increase in Eu^{3+} concentration from 0.0 mol% to 5.0 mol%. Figure 13 demonstrates how lifetime and energy transfer efficiency in co-doped BZLP glasses change when the Eu^{3+} ion concentration in the glass lattice increases.

Furthermore, on the basis of PL decay curve of BZLP:DE4, the type of energy transfer interaction has been analysed using Inokuti- Hirayama (I-H) model. As per the I-H model, the equation which relates the type of interaction as follows [44]:

$$I_t = I_0 \exp\left\{\frac{-t}{\tau_o} - Q\left(\frac{t}{\tau_o}\right)^{\frac{3}{s}}\right\} \quad (6)$$

Here I_t is intensity of luminescence at time t, τ_o signifies the decay time, Q signifies the energy transfer parameter and the value of S designates the type of interaction having values 10, 8 and 6 for quadrupole–quadrupole, dipole-quadrupole and dipole–dipole interaction, respectively [44]. The best fit is observed for $S = 6$ value as presented in Fig. 14. Thus, the I-H models also confirm the occurrence of dipole–dipole interaction among the sensitizer and activator ions in BZLP glasses.

3.7 Colorimetric analysis

Table 1 shows the CIE coordinates of the as prepared glasses. The color coordinates depend upon the incident excitation wavelength and also on the amount of dopants in the glass. Varying Eu^{3+} concentration leads to the modulation of luminescence hues and is helpful for a variety of applications. CIE chromaticity coordinates of Dy^{3+}/Eu^{3+}co-doped BZLP glasses at $\lambda_{ex} = 350$ nm correspond to the white region as seen in Fig. 15a. The coordinates for BZLP:DE5 glass at $\lambda_{ex} = 393$ nm were also plotted on the CIE diagram and shown in Fig. 15b. CIE color coordinates were situated in red region, under the $\lambda_{ex} = 393$ nm, which shows the prepared glasses can be a potential red constituent for many photonic devices.

Correlated colour temperature (CCT) is also a critical parameter which allows the researchers to determine the specific temperatures for which the CIE coordinates fall closer to the whole light region. It can be calculated using the McCamy relation [45]. The CCT values for Dy^{3+}/Eu^{3+} doped BZLP glass have been presented in Table 1 as well. The values signify emission tuning from cool to warm white light regions with the addition of Eu^{3+} ions. According to the aforementioned findings, CIE colour co-ordinates and CCT values may be effectively modified by the amount of doped RE ions BZLP glasses. In turn, this demonstrates that as-prepared Dy^{3+}/Eu^{3+} co-doped BZLP glasses are appropriate for n-UV pumped white illumination systems.

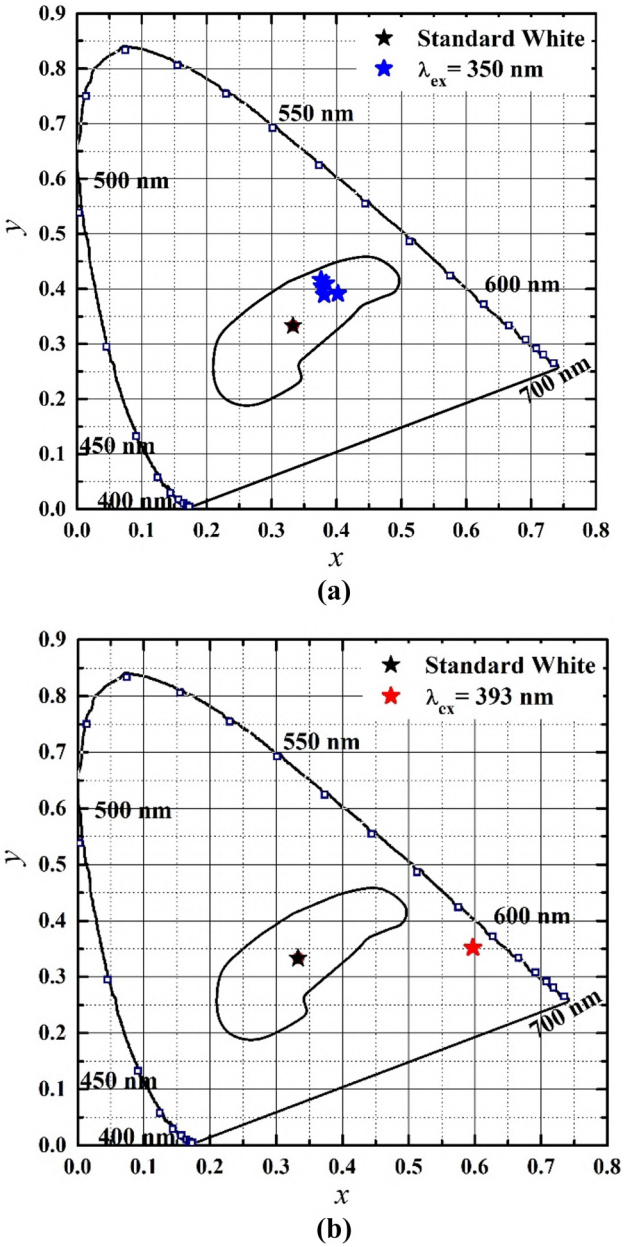

Fig. 15 CIE chromaticity coordinates of **a** Dy^{3+}/Eu^{3+}co-doped BZLP glasses at λ_{ex} = 350 nm. **b** BZLP:DE5 glass at λ_{ex} = 393 nm

3.8 Temperature dependent PL study

PL spectra are affected by variation of temperature. Hence, the temperature-dependent emission characteristics for Dy^{3+}/Eu^{3+} co-doped BZLP glass were recorded at λ_{ex} = 350 & 393 nm and shown in Fig. 16a and b. With increase in temperature from 25 to 200 °C, the PL intensity continuously decreases as can be seen in the figure. The intensity is 93.40% of maximum at 150 °C and 91.25% of maximum at 200 °C, which shows that the Dy^{3+}/Eu^{3+} co-doped BZLP glass has very good thermal stability. Furthermore, the activation energy (ΔE_a) can be accessed by using the Arrhenius equation as follows [46]:

$$I_T = \frac{I_0}{1 + Cexp\left(-\frac{\Delta E}{K_B T}\right)}$$

Here I_0 and I_T indicate the emission intensity at 25 °C and at a particular temperature T respectively whereas CandK_B signify an arbitrary constant and Boltzmann constant respectively. On the basis of temperature-dependent emission characteristics, the $ln((I_0/I_T)\text{-}1)$ versus $1/K_BT$ plots were analysed and fitted with linear equation for the both emission characteristics. The plots are shown in Fig. 17a and b. The activation energy for Dy^{3+}/Eu^{3+} co-doped BZLP glass was assessed to be 0.242 and 0.241 eV for emission spectra under λ_{ex} = 350 & 393 nm respectively which have relatively higher activation energy (0.196 eV) of reported glass in literature [3]. Thus, temperature dependent emission characteristics show that the Dy^{3+}/Eu^{3+} co-doped BZLP glass can produce thermally stable luminescence and can be used as red emitting component in w-LEDs and other luminescent devices.

4 Conclusions

Transparent Dy^{3+}/Eu^{3+} co-doped BZLP glasses were effectively synthesized via melt quench technique. The structural and luminous properties were examined to gain understanding of their applicability in photonic devices. The single Dy^{3+} doped BZLP glasses emits blue, yellow and red emission under n-UV excitation pertaining to the $^4F_{9/2} \rightarrow {}^6H_{15/2}$, $^6H_{13/2}$ and $^6H_{11/2}$ transitions respectively. Dy^{3+}/Eu^{3+} co-doped BZLP glasses give emission in visible region owing $^4F_{9/2} \rightarrow {}^6H_{15/2}$, $^6H_{13/2}$ and $^6H_{11/2}$ transitions of Dy $^{3+}$ along with $^5D_0 \rightarrow {}^7F_1$, $^5D_0 \rightarrow {}^7F_2$, $^5D_0 \rightarrow {}^7F_3$ and $^5D_0 \rightarrow {}^7F_4$ transitions of Eu $^{3+}$ ion under 350 nm and 393 nm.With an increase in Eu^{3+} ion concentration, energy transfer takes place from Dy^{3+} ions to Eu^{3+} ions resulting in the decrement of intensity of PL peaks of Dy^{3+} ions. The cool white emission shifts towards the warm white emission under 350 nm and 393 nm excitation for the co-doped glasses as can be seen in the CIE diagram.

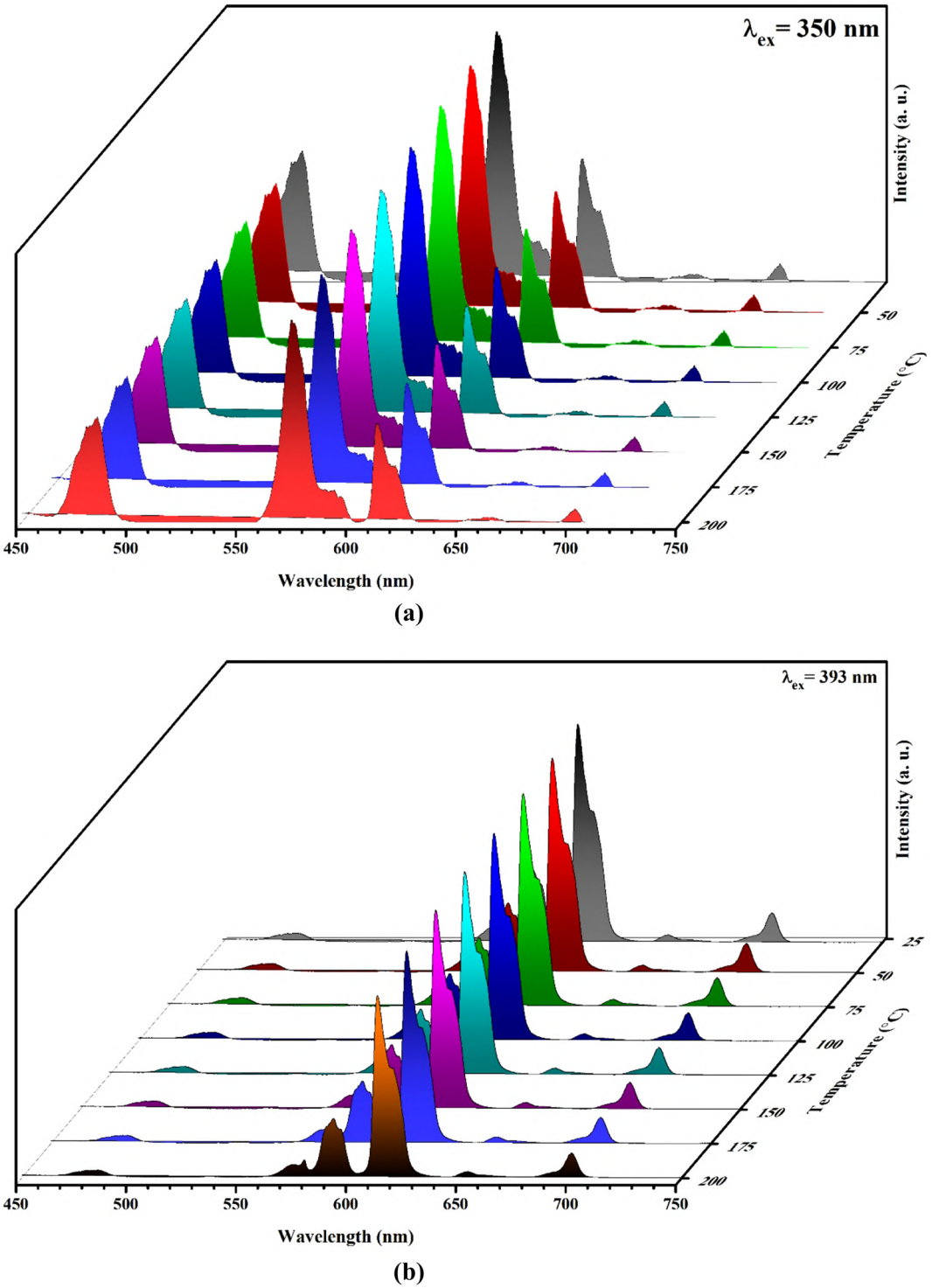

Fig. 16 Temperature dependent emission spectra of **a** BZLP:DE4 glass at $\lambda_{ex} = 350$ nm. **b** BZLP:DE5 glass at $\lambda_{ex} = 393$ nm

The dipole–dipole type of energy transfer sensitizer and activator ions in the BZLP glasses was verified using Dexter's ET formula, Reisfeld's approximation and I–H model theories. The PL lifetimes for the co-doped glasses reduced whereas the energy transfer efficiency η_T enflamed with upsurge in Eu^{3+} ions concentration from $y = 0.0$ to 5.0 mol%. The temperature-dependent PL spectra under 350 nm and 393 nm

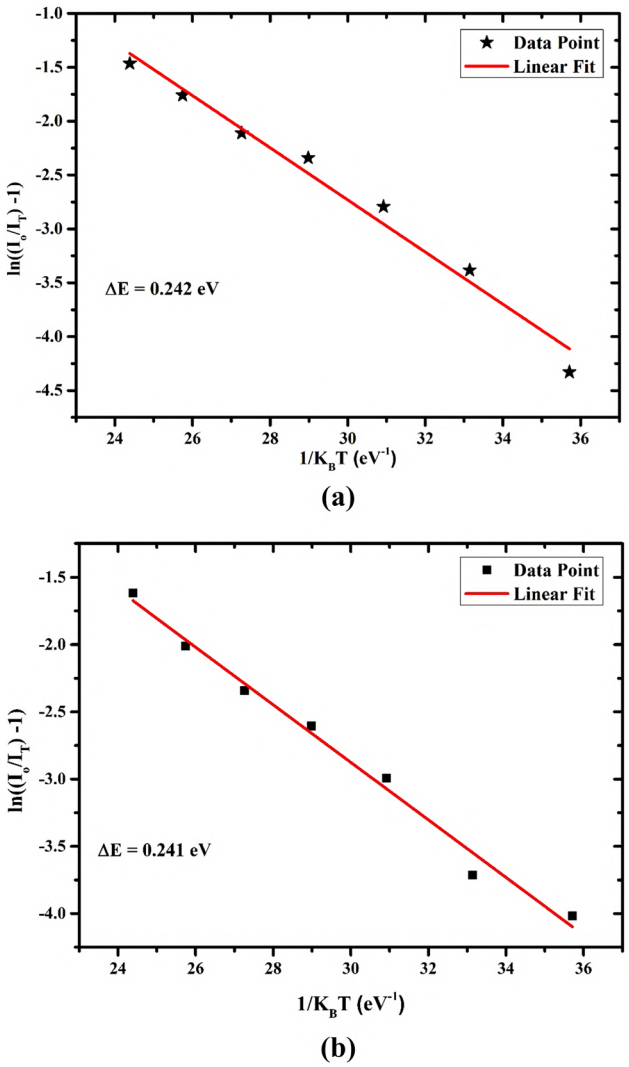

Fig. 17 $\ln[(I_0/I_T)-1]$ versus $1/K_BT$ plot for **a** BZLP:DE4 glass at $\lambda_{ex} = 350$ nm. **b** BZLP:DE5 glass at $\lambda_{ex} = 393$ nm

excitation were thermally stable with values of activation energy being 0.242 eV and 0.241 eV, respectively. The aforementioned results for Dy^{3+}/Eu^{3+} co-doped BZLP glasses show that these glasses can work is a red light emitting component in w-LEDs and for warm white light generation in various luminescent applications.

Author contributions

All authors contributed to the study, conception and design of the manuscript. The author credits are as follows: KM: Data collection, methodology, synthesis, result analysis, writing. AP: Result analysis, review, writing. RP: Result analysis, writing. SM: Result analysis. YT: Data collection, synthesis. ASR: Methodology, review, editing, supervision.

Funding

The authors declare that no funds, grants, or other support were received during the preparation of this manuscript.

Data availability

The data that support the findings of this study are not openly available due to reasons of sensitivity and are available from the corresponding author upon reasonable request.

Declarations

Competing interests The authors declare that they have no known competing financial interests or personal relationships that could have appeared to influence the work reported in this paper.

Research involving human and animal rights The authors declare that no animal or animal data was used in any study or experiment mentioned in this manuscript.

References

1. Y. Yan, Z. Chen, X. Jia, S. Li, Investigations on the effects of the Stark splitting on the fluorescence behaviors in Yb^{3+}-doped silicate, tellurite, germanate, and phosphate glasses. Opt. Mater. **75**, 465–470 (2018). https://doi.org/10.1016/j.optmat.2017.10.008
2. L. He, D. Wang, M. Chen, R. Liu, Z. Su, C. Li, H. Lin, S. Li, Y. Zhou, L. Liu, F. Zeng, Luminescence properties of Tb^{3+}/Eu^{3+} co-doped glass based on GSBR system. Opt. Mater. **122**, 111754 (2021). https://doi.org/10.1016/j.optmat.2021.111754
3. A.S. Rao, Effective energy transfer from Dy^{3+} to Tb^{3+} ions in thermally stable KZABS glasses for intense green emitting device applications. J. Lumin. **239**, 118325 (2021). https://doi.org/10.1016/j.jlumin.2021.118325

4. C. Zhang, H. Liang, S. Zhang, C. Liu, D. Hou, L. Zhou, G. Zhang, J. Shi, Efficient Sensitization of Eu^{3+} Emission by Tb^{3+} in $Ba_3La(PO_4)_3$ under VUV-UV excitation: energy transfer and tunable emission. J. Phys. Chem. C **116**, 15932–15937 (2012). https://doi.org/10.1021/jp304717z
5. N. Baig, R.S. Yadav, N.S. Dhoble, V.L. Barai, S.J. Dhoble, Near UV excited multi-color photoluminescence in RE^{3+} (RE=Tb, Sm, Dy and Eu) doped $Ca_2Pb_3(PO_4)_3Cl$ phosphors. J. Lumin. **215**, 116645 (2019). https://doi.org/10.1016/j.jlumin.2019.116645
6. C. Sumalatha, R. Doddoji, M. Venkateswarlu, P.R. Rani, K. Swapna, S. Mahamuda, A.S. Rao, White light emission from Dy^{3+}-doped ZnO+Bi_2O_3+BaF_2+$B2O_3$+TeO_2 glasses: structural and spectroscopic properties. Spectro. Acta Part A: Mol. Biomol. Spectrosc. **240**, 118568 (2020). https://doi.org/10.1016/j.saa.2020.118568
7. P.R. Rani, M. Venkateswarlu, S. Mahamuda, K. Swapna, N. Deopa, A.S. Rao, Spectroscopic studies of Dy^{3+} ions doped barium lead alumina fluoro borate glasses. J. Alloys Compd. **787**, 503–518 (2019). https://doi.org/10.1016/j.jallcom.2019.02.088
8. H. Bouchouicha, G. Panczer, D. De Ligny, Y. Guyot, M.L. Baesso, L.H. Andrade, S.M. Lima, R. Ternane, Synthesis and luminescent properties of Eu^{3+}/Eu^{2+} co-doped calcium aluminosilicate glass–ceramics. J. Lumin. **169**, 528–533 (2016). https://doi.org/10.1016/j.jlumin.2014.11.054
9. A.S. Rao, R.R. Reddy, T.R. Rao, J.L. Rao, Electron paramagnetic resonance and optical absorption spectra of Fe^{3+} ions in alkali cadmium borosulphate glasses. Solid State. Comm. **96**, 701–705 (1995). https://doi.org/10.1016/0038-1098(95)00375-4
10. B.H. Babu, V.R.K. Kumar, White light generation in $Ce^{3+}Tb^{3+}$ Sm^{3+} codoped oxyfluoroborate glasses. J. Lumin **154**, 334–338 (2014). https://doi.org/10.1016/j.jlumin.2014.05.010
11. S. Ye, F. Xiao, Y.X. Pan, Y.Y. Ma, Q.Y. Zhang, Phosphors in phosphor-converted white light-emitting diodes: recent advances in materials, techniques and properties. Mater. Sci. Eng. **71**(1), 1–34 (2010). https://doi.org/10.1016/j.mser.2010.07.001
12. H. Masai, Y. Yamada, Y. Suzuki, K. Teramura, Y. Kanemitsu, T. Yoko, Narrow energy gap between triplet and singlet excited states of Sn21 in borate glass. Sci. Rep. **3**, 3541 (2013). https://doi.org/10.1038/srep03541
13. N. Deopa, S. Saini, S. Kaur, A. Prasad, A.S. Rao, Spectroscopic investigations on Dy^{3+} ions doped zinc lead alumino borate glasses for photonic device applications. J. Rare Earths **37**, 52–59 (2019). https://doi.org/10.1016/j.jre.2018.04.013
14. N. Deopa, A.S. Rao, S.K. Mahamuda, M. Gupta, M. Jayasimhadri, D. Haranath, G. Vijaya Prakash, Spectroscopic studies of Pr3+ doped lithium lead alumino borate glasses for visible reddish orange luminescent device applications. J. Alloys Compd. **708**, 911–921 (2017). https://doi.org/10.1016/j.jallcom.2017.03.020
15. G. Lakshminarayana, S. Buddhudu, Spectral analysis of Eu^{3+} and Tb^{3+}:B_2O_3–ZnO–PbO glasses. Mater. Chem. Phys. **102**, 181–186 (2007). https://doi.org/10.1016/j.matchemphys.2006.11.020
16. R.J. Amjad, M.R. Dousti, M.R. Sahar, Spectroscopic investigation and Judd-Ofelt analysis of silver nanoparticles embedded Er^{3+}-doped tellurite glass. Curr. Appl. Phys. **15**, 1–7 (2015). https://doi.org/10.1016/j.cap.2014.10.022
17. M. Higuchi, R. Sasaki, J. Takahashi, Float zone growth of Dy:$GdVO_4$ single crystals for potential use in solid-state yellow lasers. J. Cryst. Growth **311**, 4549–4552 (2009). https://doi.org/10.1016/j.jcrysgro.2009.08.028
18. K. Siva Rama Krishnareddy, K. Swapna, S.K. Mahamuda, M. Venkateswarlu, A.S. Rao, G. Vijayaprakash, Investigation on structural and luminescence features of Dy^{3+} ions doped alkaline-earth boro tellurite glasses for optoelectronic devices. Opt. Mater. **85**, 200–210 (2018). https://doi.org/10.1016/j.optmat.2018.08.057
19. P. Manasa, C.K. Jayasankar, Spectroscopic assessment of Dy^{3+} ions in lead fluorosilicate glass as a prospective material for solid state yellow laser, Spectrochim. Acta - Part A Mol. Biomol. Spectrosc. **212**, 315–321 (2019). https://doi.org/10.1016/j.saa.2019.01.015
20. Q. Luo, X. Qiao, X. Fan, H. Yang, X. Zhang, S. Cui, L. Wang, G. Wang, Luminescence behavior of Ce^{3+} and Dy^{3+} codoped oxyfluoride glasses and glass ceramics containing LaF_3 nanocrystals. J. Appl. Phys. **105**(043506), 1–5 (2009). https://doi.org/10.1063/1.3077266
21. N. Deopa, A.S. Rao, Spectroscopic studies of single near ultraviolet pumped Tb^{3+} doped Lithium Lead Alumino Borate glasses for green lasers and tricolour w-LEDs. J. Lumin. **194**, 56–63 (2018). https://doi.org/10.1016/j.jlumin.2017.09.057
22. A. Vidhi, Anu, AS Rao, Spectroscopic characterizations of Dy^{3+} ions doped phosphate glasses for epoxy-free white LED applications. Opt. Mater. **132**, 112863 (2022). https://doi.org/10.1016/j.optmat.2022.112863
23. Y. Tayal, A.S. Rao, Spectroscopic analysis of Dy^{3+} ions activated borosilicate glasses for photonic device applications. Opt. Mater. **117**, 111112 (2021). https://doi.org/10.1016/j.optmat.2021.111112
24. Z. Zhu, Y. Zhang, Y. Qiao, H. Liu, D. Liu, Luminescence properties of Ce^{3+}/Tb^{3+}/Sm^{3+} co-doped CaO–SiO_2–B_2O_3

glasses for white light emitting diodes. J. Lumin. **134**, 724–728 (2013). https://doi.org/10.1016/j.jlumin.2012.07.003

25. A. Ravita, P. Prasad, A. Rohilla, A.S. Shandilya, Rao, Photoluminescence and energy transfer studies on Tm^{3+}/Dy^{3+}/Eu^{3+}doped borosilicate glasses for color tunability and warm white light generation. J. Non-Cryst. Solids **606**, 122192 (2023). https://doi.org/10.1016/j.jnoncrysol.2023.122192
26. U. Caldino, A. Speghini, E. Alvarez, S. Berneschi, M. Bettinelli, M. Brenci, G.C. Righini, Spectroscopic characterization and optical waveguide fabrication in Ce^{3+}, Tb^{3+} and Ce^{3+}/Tb^{3+} doped zinc–sodium–aluminosilicate glasses. Opt. Mater. **33**(12), 1892–1897 (2011). https://doi.org/10.1016/j.optmat.2011.03.012
27. N. Deopa, M.K. Sahu, P.R. Rani, R. Punia, A.S. Rao, Realization of warm white light and energy transfer studies of Dy^{3+}/Eu^{3+} co-doped Li_2O-PbO-Al_2O_3-B_2O_3 glasses for lighting applications. J. Lumin. **222**, 117166 (2020). https://doi.org/10.1016/j.jlumin.2020.117166
28. G. Lakshminarayana, H.C. Yang, J.R. Qiu, White light emission from Tm^{3+}/Dy^{3+} co-doped oxyfluoride germanate glasses under UV light excitation. J. Solid State Chem. **182**, 669–676 (2009). https://doi.org/10.1016/j.jssc.2008.11.020
29. E.A. Davis, N.F. Mott, Conduction in non-crystalline systems V. Conductivity, optical absorption and photoconductivity in amorphous semiconductors. Philos. Mag. **22**, 903–922 (1970). https://doi.org/10.1080/14786437008221061
30. A. Agarwal, V.P. Seth, S. Sanghi, P. Gahlot, D.R. Goyal, Optical band gap studies and estimation of two photon absorption coefficient in alkali bismuth borate glasses. Radiat. Eff. Defects Solids **158**, 793–801 (2003). https://doi.org/10.1080/10420150310001618214
31. P. Borisut, S. Insiripong, P. Limkitjaroenporn, P. Meejitpaisan, E. Kaewnuam, W. Chaipaksa, R. Rajaramakrishna, H.J. Kim, J. Kaewkhao, Luminescence and Judd-Ofelt analysis of gallium aluminum gadolinium yttrium borate scintillating glass doped with Dy^{3+}. Radiat. Phys. Chem. **199**, 110284 (2022). https://doi.org/10.1016/j.radphyschem.2022.110284
32. A.R. Venugopal, R. Rajaramakrishna, K.M. Rajashekara, J. Rajaguguk, N.H. Ayachit, S. Kothan, J. Kaewkhao, Dy^{3+} doped B_2O_3 – Li_2O – CaO – CaF_2 glass for efficient white light emitting sources. J. Non-Cryst. Solids **554**, 120604 (2021). https://doi.org/10.1016/j.jnoncrysol.2020.120604
33. N. Wantana, Y. Ruangtaweep, E. Kaewnuam, S.C. Kang, H.J. Kim, S. Kothan, J. Kaewkhao, Development of WO_3-Gd_2O_3- B_2O_3 high density glasses doped with Dy^{3+} for photonics and scintillation materials application. Solid State Sci. **101**, 106135 (2020). https://doi.org/10.1016/j.solidstatesciences.2020.106135
34. K. Maheshwari, A.S. Rao, Photoluminescence downshifting studies of thermally stable Dy^{3+} ions doped phosphate glasses for photonic device applications. Opt. Mater. **129**, 112518 (2022). https://doi.org/10.1016/j.optmat.2022.112518
35. M. Seshadri, M.J.V. Bell, V. Anjos, Y. Messaddeq, Influence of silver ions in Eu^{3+} doped glass for efficient reddish-orange and white light generation. J. Alloy. Compd. **838**, 155548 (2020). https://doi.org/10.1016/j.jallcom.2020.155548
36. D. Rajesh, K. Brahmachary, Y.C. Ratnakaram, N. Kiran, A.P. Baker, G.G. Wang, Energy transfer based emission analysis of Dy^{3+}/Eu^{3+} co-doped ZANP glasses for white LED applications. J. Alloys Compd. **646**, 1096–1103 (2015). https://doi.org/10.1016/j.jallcom.2015.05.138
37. D.A. Rodríguez-Carvajal, A.N. Meza-Rocha, U. Caldino, R. Lozada-Morales, E. Alvarez, Reddish-orange, neutral and warm white emissions in Eu^{3+}, Dy^{3+} and Dy^{3+}/Eu^{3+} doped CdO-GeO_2-TeO_2 glasses. Ma. Solid State Sci. **61**, 70–76 (2016). https://doi.org/10.1016/j.solidstatesciences.2016.09.009
38. T.A. Lodi, M. Sandrini, A.N. Medina, M.J. Barboza, F. Pedrochi, A. Steimacher, Dy: Eu doped CaBAl glasses for white light applications. Opt. Mater. **76**, 231–236 (2018). https://doi.org/10.1016/j.optmat.2017.12.043
39. Y. Tayal, A.S. Rao, S. Kaur, Photoluminescence characteristics of Sm^{3+}/Eu^{3+} co-doped LPZABS glasses for solar cell applications. Solid State Sci. **125**, 106834 (2022). https://doi.org/10.1016/j.solidstatesciences.2022.106834
40. K. Li, X. Liu, Y. Zhang, X. Li, H. Lian, J. Lin, Host-sensitized luminescence properties in $CaNb_2O_6$:Ln^{3+} (Ln^{3+} = Eu^{3+}/Tb^{3+}/Dy^{3+}/Sm^{3+}) phosphors with abundant colors. Inorg. Chem. **54**(1), 323–333 (2015). https://doi.org/10.1021/ic502493c
41. F. Kang, Y. Zhang, M. Peng, Controlling the energy transfer via multi luminescent centers to achieve white light/tunable emissions in a single-phased X2-Type Y_2SiO_5:Eu^{3+}, Bi^{3+} phosphor for ultraviolet converted LEDs. Inorg. Chem. **54**, 1462–1473 (2015). https://doi.org/10.1021/ic502439k
42. L. Mishra, A. Sharma, A.K. Vishwakarma, K. Jha, M. Jayasimhadri, B.V. Ratnam, K. Jang, A.S. Rao, R.K. Sinha, White light emission and color tunability of dysprosium doped barium silicate glasses. J. Lumin. **169**, 121–127 (2016). https://doi.org/10.1016/j.jlumin.2015.08.063
43. X. Min, Z. Huang, M. Fang, Y. Liu, C. Tang, X. Wu, Energy transfer from Sm^{3+} to Eu^{3+} in red-emitting phosphor $LaMgAl_{11}O_{19}$:Sm^{3+}, Eu^{3+} for solar cells and

near-ultraviolet white light-emitting diodes. Inorg. Chem. **53**, 6060–6065 (2014). https://doi.org/10.1021/ic500412r

44. S. Kaur, N. Deopa, A. Prasad, R. Bajaj, A.S. Rao, Intense green emission from Tb^{3+} ions doped zinc lead alumino borate glasses for laser and w-LED applications. Opt. Mater. **84**, 318–323 (2018). https://doi.org/10.1016/j.optmat.2018.07.020
45. C.S. McCamy, Correlated color temperature as an explicit function of chromaticity coordinates. Color. Res. Appl. **17**, 142–144 (1992). https://doi.org/10.1002/col.5080170211
46. P. Li, M. Peng, X. Yin, Z. Ma, G. Dong, Q. Zhang, J. Qiu, Temperature dependent red luminescence from a distorted Mn^{4+} site in $CaAl_4O_7$:Mn4+. Express. **21**, 18943–18948 (2013). https://doi.org/10.1364/OE.21.018943